Proceedings of the ASME 2015 Dynamic Systems and Control Conference
DSCC2015
October 28-30, 2015, Columbus, Ohio, USA

DSCC2015-9699

A DIAGNOSTIC SCHEME FOR DETECTION, ISOLATION AND ESTIMATION OF ELECTROCHEMICAL FAULTS IN LITHIUM-ION CELLS

Satadru Dey
Clemson University
Greenville, SC-29607, USA
satadrd@clemson.edu

Beshah Ayalew
Clemson University
Greenville, SC-29607, USA
beshah@clemson.edu

ABSTRACT

Improvement of the safety and reliability of the Lithium-ion (Li-ion) battery operation is one of the key tasks for advanced Battery Management Systems (BMSs). It is critical for BMSs to be able to diagnose battery electrochemical faults that can potentially lead to catastrophic failures. In this paper, an observer-based fault diagnosis scheme is presented that can detect, isolate and estimate some internal electrochemical faults. The scheme uses a reduced-order electrochemical-thermal model for a Li-ion battery cell. The paper first presents a modeling framework where the electrochemical faults are modeled as parametric faults. Then, multiple sliding mode observers are incorporated in the diagnostic scheme. The design and selection of the observer gains as well as the convergence of the observers are verified theoretically via Lyapunov's direct method. Finally, the performance of the observer-based diagnostic scheme is illustrated via simulation studies.

NOMENCLATURE

A	Current collector area (cm^2)
$a_s^{\pm}$	Specific surface area (cm^2/cm^3)
c_e	Electrolyte phase Li-ion concentration (mol/cm^3)
$c_s^{\pm}$	Solid phase Li-ion concentration (mol/cm^3)
$c_{s,e}^{\pm}$	Solid-phase Li-ion surface-concentration (mol/cm^3)
$c_{s,max}^{\pm}$	Solid-phase Li-ion max. concentration (mol/cm^3)
$D_s^{\pm}$	Diffusion coefficient in solid phase (cm^2/s)
$D_{s,ref}^{\pm}$	Diffusion coefficient at T_{ref} (cm^2/s)
$E_K^{\pm}$	Activation Energy of diffusion coefficient (J/mol)
$E_{Ds}^{\pm}$	Activation Energy of reaction rate constant (J/mol)
E_R	Activation Energy of contact film resistance (J/mol)
K_h	Heat transfer coefficient of the cell (W/ K)
F	Faraday's constant (C/mol)
I	Current (A)
$K^{\pm}$	Reaction rate constant ($cm^{2.5}/mol^{0.5}/s$)
$K_{ref}^{\pm}$	Reaction rate constant at T_{ref} ($cm^{2.5}/mol^{0.5}/s$)
$L^{\pm}$	Length of the cell (cm)
r	Radial coordinate (cm)
$R^{\pm}$	Radius of solid active particle (cm)
$\bar{R}$	Universal Gas Constant (J/mol-K)
$R_{f,ref}$	Contact resistance (Ω)
T	Temperature (K)
T_{ref}	Reference temperature (K)
T_{amb}	Temperature of cooling fluid (K)
$U^{\pm}$	Open circuit potential (V)
$\alpha^{\pm}$	Charge transfer coefficient
ρ	Cell density (g/cm^3)
v	Cell volume (cm^3)
C_p	Specific heat capacity (J/g-K)
$\varepsilon_s^{\pm}$	Active material volume fraction (-)

Superscript

$\pm$	positive/negative electrode

INTRODUCTION

Despite beneficial features such as higher power-to-weight ratio, low self-discharge, Lithium-ion (Li-ion) batteries still suffer from the issues of safety, reliability and longevity. This motivates the need for advanced Battery Management Systems (BMSs) that improve the battery operation via safe and intelligent management. These BMS must have the capability to detect different kind of battery failures in order to maintain a reliable and safe operation. Various fault mechanisms can degrade the battery performance and safety, spanning from internal electrochemical failure to sensor and actuator faults. Some of these failures may even lead to catastrophic failures. Therefore, early and real-time detection of these failures could be beneficial in replacing the faulty battery or taking other fault-tolerant actions to prevent catastrophic outcomes. Motivated by this scenario, we propose a real-time diagnostic

scheme in this paper that addresses the diagnosis of electrochemical faults in a Li-ion battery cell.

In the existing literature, real-time state and parameter estimation problems for Li-ion batteries are well studied. Based on the kind of model used, these estimation approaches can be classified as: 1) Data-driven model-based [1-2], 2) Equivalent circuit model-based (ECM) [3-4], and 3) Electrochemical model-based [5-12]. The authors of the present paper have proposed electrochemical model-based algorithms for state and/or parameter estimation of Li-ion batteries [13-16].

Other than estimating the states and parameters of the nominal battery models, the BMS should also have the capabilities for diagnosing different faults in the batteries. However, unlike the estimation problem, the real-time fault diagnosis problem for Li-ion batteries has received less emphasis in the current literature. In [17][18], a review of Li-ion battery failure mechanisms was presented. The diagnostics related challenges for Li-ion batteries were described in [19]. In [20], a diagnostic scheme was presented for sensor and actuation faults via a combination of open-loop models and sliding mode observers. In [21], an algorithm was presented that detects over-charge and over-discharge faults using Kalman filter based multiple-model adaptive estimation. Another algorithm for detecting and predicting terminal voltage collapses was presented in [22] that uses a universal adaptive stabilization technique. In [23], an observer-based scheme was proposed for fault isolation and estimation in a faulty cell in a battery string. In [24], sensor fault diagnosis algorithms are presented for a battery pack. In [25], structural analysis and sequential residual generation technique was presented for fault diagnosis of Li-ion batteries. In [26], an electrochemical model-based diagnostic algorithm was presented for Li-ion plating detection. A side reaction current density estimation algorithm was presented based on retrospective cost subsystem identification in [27]. The authors of the present paper have also proposed a sliding-mode observer based sensor fault detection and estimation strategy in [28]. Some data-driven methods are presented for battery diagnostics in [29-31]. However, the main drawbacks for data-driven approaches are the requirement of extensive data that captures various fault scenarios and lack of physical meaning of the model variables. In [32], a fuzzy-logic based scheme that uses an electrochemical model was presented for detecting battery faults such as over-charge, over-discharge and degradation.

However, most of the afore-mentioned diagnostic schemes have one or more of the following issues: 1) focused on sensor faults alone, 2) concentrated on one particular fault, 3) rely on equivalent circuit model that has limited capabilities to capture electrochemical faults. Moreover, most of the approaches do not use electrochemical models, which are arguably more accurate than others in capturing internal electrochemical phenomena [33]. Although an electrochemical model was used in [26], [27], they concentrate on very specific fault mechanisms. The approach in [32] detects battery degradation in general but does not isolate or estimate specific electrochemical faults.

In this paper, we contribute to this area of research by proposing a coupled electrochemical-thermal model-based algorithm that can potentially diagnose various electrochemical faults. Specifically, in our approach, we take into account various electrochemical faults and propose 1) a *modeling framework* for them based on existing reduced-order electrochemical-thermal models [7], [8], and, 2) a scheme for detecting, and then isolating specific types of fault, and also providing an estimate of the fault. In our modeling framework, various electrochemical faults are modeled as parametric faults in the system. Few estimation approaches exist in the literature that estimate some electrochemical parameters in order to track battery ageing under the assumption that those parameters change in a much slower time-scale. Here we consider parametric deviations from a fault diagnosis perspective, which allows capturing the fast time-scale battery internal faults in addition to the slow time-scale ageing effect. In our diagnostic scheme, we design an observer-based algorithm that uses a set of sliding mode observers to detect, isolate and estimate various electrochemical faults. We also provide an analytical proof of the convergence of the overall observer-based scheme via Lyapunov's stability analysis. Sliding mode methodology [34] is chosen for the observer design due to the possibility to reconstruct the faults via *equivalent output error injection*, which is a filtered version of the switching feedback term in the observer [35].

The rest of the paper is organized as follows. The next section discusses the electrochemical-thermal model of Li-ion cell along with the fault-modeling framework. Then, a detailed description of the proposed fault diagnosis scheme is provided. This is followed by simulation results that illustrate the performance of the proposed scheme and concluding remarks.

SYSTEM MODELING

Reduced Order Electrochemical-thermal Model of Li-ion Cell

In this section, we will discuss an existing reduced order nominal (non-faulty) electrochemical-thermal model of Li-ion cell known as the Single Particle Model (SPM) [7], [8]. The SPM comprises of two linear Li-ion diffusion PDEs given by (1) and a nonlinear voltage equation given by (2).

$$\frac{\partial c_s^{\pm}}{\partial t} = \frac{D_s^{\pm}(T)}{r^2}\frac{\partial}{\partial r}\left(r^2\frac{\partial c_s^{\pm}}{\partial r}\right)$$
$$\left.\frac{\partial c_s^{\pm}}{\partial r}\right|_{r=0} = 0, \qquad \left.\frac{\partial c_s^{\pm}}{\partial r}\right|_{r=R^{\pm}} = \frac{\pm I}{a_s^{\pm} F D_s^{\pm}(T) A L^{\pm}} \tag{1}$$

$$V = \frac{\bar{R}T}{\alpha^{+}F}sinh^{-1}\left(\frac{I}{2a_s^{+}AL^{+}K^{+}(T)\sqrt{c_e c_{s,e}^{+}\left(c_{s,max}^{+} - c_{s,e}^{+}\right)}}\right) - \frac{\bar{R}T}{\alpha^{-}F}sinh^{-1}\left(\frac{I}{2a_s^{-}AL^{-}K^{-}(T)\sqrt{c_e c_{s,e}^{-}\left(c_{s,max}^{-} - c_{s,e}^{-}\right)}}\right) + U^{+}\left(c_{s,e}^{+},T\right) - U^{-}\left(c_{s,e}^{-},T\right) - R_f(T)I \tag{2}$$

where $U^{\pm}$ are the thermodynamic potentials of the electrodes, $c_s^{\pm}$ is the Li-ion concentration of the electrodes, $a_s^{\pm} = 3/R^{\pm}$ is the active surface area, V is the voltage and I is the current. Rest of the variables is defined in the nomenclature section. Next, the following lumped thermal dynamics is adopted [36]:

$$\rho v C_p \frac{dT}{dt} = I\left(U^+(c_{s,e}^+, T) - U^-(c_{s,e}^-, T) - V - T\left(\frac{\partial U^+}{\partial T} - \frac{\partial U^-}{\partial T}\right)\right) - K_h(T - T_{amb}) \quad (3)$$

where T is the lumped averaged temperature of the cell and $\partial U^{\pm}/\partial T$ are the changes in thermodynamic potentials due to temperature. Some electrochemical parameters possess Arrhenius' type dependence on temperature. For example, solid phase diffusion coefficients ($D_s^{\pm}$), the reaction rate constants ($K^{\pm}$) and film resistance (R_f):

$$K^{\pm}(T) = K_{ref}^{\pm}\exp\left(\frac{E_K^{\pm}}{\bar{R}}\left(\frac{1}{T} - \frac{1}{T_{ref}}\right)\right)$$
$$D_s^{\pm}(T) = D_{s,ref}^{\pm}\exp\left(\frac{E_{Ds}^{\pm}}{\bar{R}}\left(\frac{1}{T} - \frac{1}{T_{ref}}\right)\right)$$
$$R_f(T) = R_{f,ref}\exp\left(\frac{E_R}{\bar{R}}\left(\frac{1}{T} - \frac{1}{T_{ref}}\right)\right) \quad (4)$$

with T_{ref} as temperature reference, $K_{ref}^{\pm}$, $D_{s,ref}^{\pm}$ and $R_{f,ref}$ are reference values at the reference temperature. Further, the following approximation of the thermodynamic potential expression is adopted [36]:

$$U^{\pm}(c_{s,e}^{\pm}, T) \approx U^{\pm}(c_{s,e}^{\pm}, T_{ref}) + \frac{\partial U^{\pm}}{\partial T}(T - T_{ref}) \quad (5)$$

Note: In the existing literature, some modeling approaches exist that extend the conventional SPM and the averaged thermal model, e.g. [37] and [38]. However, the present paper only illustrates the electrochemical fault diagnosis approach using the conventional SPM and lumped averaged thermal model. Extension of the approach using the enhanced models can be considered a future work of this study.

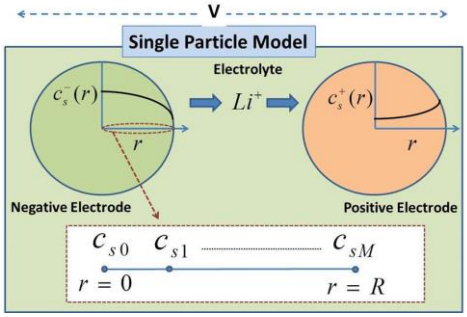

Figure 1: Illustration of SPM with Discretized Nodes

The SPM states are weakly observable from the measured voltage [8]. To get an observable model, the positive electrode concentration is approximated as an algebraic function of the negative electrode concentration based on the conservation of Li-ions [9]. With this step, we now have one PDE describing Li-ion diffusion dynamics in the negative electrode and a nonlinear output voltage function. Next, the PDE is discretized by defining a set of nodes $[c_{s0}, c_{s1}, \dots c_{sM}]$ along the radius of the negative electrode particle as shown in Fig. 1. Then the spatial derivatives are approximated via the central in space finite difference method leading to a set of ODEs given in (6).

$$\begin{aligned}
\dot{c}_{s0} &= -3ac_{s0} + 3ac_{s1}\\
\dot{c}_{sm} &= \left(1 - \frac{1}{m}\right)ac_{s(m-1)} - 2ac_{sm} + \left(1 + \frac{1}{m}\right)ac_{s(m+1)}\\
\dot{c}_{sM} &= \left(1 - \frac{1}{M}\right)ac_{s(M-1)} - \left(1 - \frac{1}{M}\right)ac_{sM} - \left(1 + \frac{1}{M}\right)bI
\end{aligned} \quad (6)$$

with $m = 1, \dots, (M-1)$, discretization step $\Delta = R^-/M$, $a = D_s^-/\Delta^2$, $b = 1/a_s^- F\Delta A L^-$. The output voltage expression and thermal dynamics can be re-written from (2) and (3) respectively, by substituting $c_{s,e}^- = c_{sM}$ and $c_{s,e}^+ = k_1 c_{sM} + k_2$. Note that, k_1 and k_2 are constants in the algebraic relationship between positive and negative electrode Li-ion concentrations that are derived based on conservation of Li-ions in the cell [9].

State-space Model Formulation

Considering (6) and (2), the electrochemical state-space model for the Li-ion cell can be written as:

$$\begin{aligned}
\dot{x} &= f_1(T)\theta A x + Bu\\
y &= h(x_M, T) + \eta(x_M, T, u) - R_{f,ref} f_2(T) u
\end{aligned} \quad (7)$$

where $x = [c_{s1}, \dots, c_{sM}]^T \in \mathbb{R}^M$ is the state vector describing Li-ion concentrations at various nodes, $x_M = x(M) = c_{sM} \in \mathbb{R}$ is the surface concentration state, $A \in \mathbb{R}^{M\times M}$ is a tri-diagonal matrix derived from (6), $\theta = D_{s,ref}^-/\Delta^2 \in \mathbb{R}$ is the scalar parameter related to the diffusion coefficient, $B = [0, \dots, 0, B_M]^T \in \mathbb{R}^{M\times 1}$ is a column vector formed from (6) where $B_M = 1/a_s^- F\Delta A L^-$, $R_{f,ref} \in \mathbb{R}$ is the reference contact resistance, $y \in \mathbb{R}$ is the measured voltage, $u \in \mathbb{R}$ is the input current, $f_1, f_2 : \mathbb{R} \to \mathbb{R}$ are scalar functions of the temperature given by the exponential term in the Arrhenius relations (4), $h = (U^+ - U^-) : \mathbb{R}^2 \to \mathbb{R}$ is a scalar function derived from the thermodynamic potentials of the electrodes, $\eta : \mathbb{R}^3 \to \mathbb{R}$ is a scalar function derived from the first two hyperbolic sine inverse terms in the RHS of (2). Now, we are going to write the state equation in (7) in a partitioned form with $x = [x_1 \quad x_M]^T$ where $x_M \in \mathbb{R}$ is the surface concentration state and $x_1 = [c_{s1}, \dots, c_{s(M-1)}]^T \in \mathbb{R}^{M-1}$ is the partial state vector containing the concentrations at the rest of the spatial nodes. Based on this, the A and B matrices in (7) can also be written in partitioned form as: $A = \begin{bmatrix} A_{11} & A_{12} \\ A_{21} & A_{22} \end{bmatrix}$ where $A_{11} \in \mathbb{R}^{(M-1)\times(M-1)}$, $A_{12} \in \mathbb{R}^{(M-1)\times 1}$, $A_{21} \in \mathbb{R}^{1\times(M-1)}$, $A_{22} \in \mathbb{R}$ and $B = \begin{bmatrix} O \\ B_M \end{bmatrix}$ where $O \in \mathbb{R}^{(M-1)\times 1}$ is a vector containing zeros and $B_M \in \mathbb{R}$ as defined above. Therefore, the state equation can be written in partitioned form as:

$$\dot{x}_1 = f_1(T)\theta(A_{11}x_1 + A_{12}x_M) \quad (8)$$

$$\dot{x}_M = f_1(T)\theta(A_{21}x_1 + A_{22}x_M) + B_M u \quad (9)$$

$$y = h(x_M, T) + \eta(x_M, T, u) - R_{f,ref} f_2(T) u \quad (10)$$

This partitioned form will be used for observer design later.

Now considering (3), the state-space form of the thermal model can be written as:

$$\rho v C_p \dot{T} = -K_h(T - T_{amb}) + u\{h(x_M, T) - y - Th_d\} \quad (11)$$

where $h_d = \left(\frac{\partial U^+}{\partial T} - \frac{\partial U^-}{\partial T}\right)$. We shall denote the thermal model in (11) as *Thermal Model I*. From the voltage equation in (10):

$$\begin{aligned} &y = h(x_M, T) + \eta(x_M, T, u) - R_{f,ref} f_2(T) u \\ &\Rightarrow h(x_M, T) - y = -\eta(x_M, T, u) + R_{f,ref} f_2(T) u \end{aligned} \quad (12)$$

Using (11) and (12), another formulation of the thermal model (*Thermal Model II*) can be written as:

$$\begin{aligned} &\rho v C_p \dot{T} = -K_h(T - T_{amb}) \\ &+u\{-\eta(x_M, T, u) + R_{f,ref} f_2(T) u - Th_d\} \end{aligned} \quad (13)$$

Note that the two formulations are equivalent and capture the same thermal dynamics of the cell. Note that the difference between these formulations is that (11) contains the open-circuit thermodynamic potential ($h(x_M, T)$) information and (13) contains the contact resistance ($R_{f,ref}$) information. These two formulations will be used later in the observer design section.

Modeling of Electrochemical Faults

A partial list of different electrochemical faults is discussed in [19], some of which are: Electrical contact loss, damage in current collector, Solid-Electrolyte Interface (SEI) growth, structural fracture of the electrodes, Lithium plating, negative electrode diffusion coefficient decrease, change in electrode porosity, particle size change etc. As can be seen from the above list, the electrochemical faults follow a wide spectrum of physical phenomena and it is very difficult to capture the effect of all of them in a single modeling framework. Moreover, for real-time implementable model-based diagnostic schemes, there is a trade-off between the acceptable complexity of the model and its predictive capability. In this paper, we attempt to address this trade-off by proposing a modeling strategy for electrochemical faults with respect to already existing, reduced-order and real-time suitable SPM extended with the lumped thermal models as discussed in the previous section.

The modeling strategy is based on the parametric/multiplicative fault models commonly used in the fault diagnosis literature [39]. The parametric/multiplicative fault modeling is based on the observation that often the occurrence of a fault manifests itself as a change in the values of one or more parameters of the system and so the fault is best modeled as deviation in one or more of these parameters. In this paper, we adopt a similar approach to describe the electrochemical faults as deviations in the parameters of the SPM plus thermal model. In line with this discussion, some of the afore-mentioned electrochemical faults and their effects on the different SPM parameters in (8)-(10), are given as :i) The fault {Decrease in diffusion coefficient} affects the parameter θ. ii) The faults {Change in particle size, change in porosity etc.} affect the parameter B_M. Note that, θ is also affected by change in SPM model particle size R^-, however, the effect of this may be minimized by a choice of finer discretization (higher value of M). As will be shown later, this is required for the isolation of faults in θ and B_M. iii) The faults {electrical contact loss, damage in current collector, SEI growth etc.} affect the parameter $R_{f,ref}$.

These modeled faults can be incorporated in the electrochemical and thermal models as follows.

Electrochemical Model:

$$\dot{x}_1 = f_1(T)(\theta + \theta_F)(A_{11}x_1 + A_{12}x_M) \quad (14)$$

$$\begin{aligned} \dot{x}_M = f_1(T)(\theta + \theta_F)(A_{21}x_1 + A_{22}x_M) \\ + (B_M + B_F)u \end{aligned} \quad (15)$$

$$y = h(x_M, T) + \eta(x_M, T, u) - \left(R_{f,ref} + R_F\right) f_2(T) u \quad (16)$$

Thermal Model I:

$$\rho v C_p \dot{T} = -K_h(T - T_{amb}) + u\{h(x_M, T) - y - Th_d\} \quad (17)$$

Thermal Model II:

$$\begin{aligned} &\rho v C_p \dot{T} = -K_h(T - T_{amb}) \\ &+u\{-\eta(x_M, T, u) + \left(R_{f,ref} + R_F\right) f_2(T) u - Th_d\} \end{aligned} \quad (18)$$

where θ_F, B_F and R_F are the parametric/multiplicative faults. Note that with this modeling of faults, we will only be able to diagnose θ_F, B_F and R_F, not the exact phenomenon behind them such as change in particle size or change in porosity. To determine the exact electrochemical phenomenon, offline electrochemical *in-situ* studies can be conducted [40].

In the existing fault diagnosis literature, faults are classified based on their frequency domain characteristics: 1) *abrupt* or jump-type faults, that represent sudden changes and modelled as step functions, 2) *incipient* or drift-like faults, that represent slow changes and can be modelled as ramp functions [39]. In the context to battery electrochemical faults, we can use this classification to separate two different types of faults: 1) aging-related faults can be considered as *incipient* faults which are generally much slower in nature than the inherent system dynamics, and 2) faults that are not related to cycle/calendar aging but can occur due to some sudden electrochemical and/or thermal reactions inside the cell owing to abnormal operating conditions or abuse. This type of failures can be considered as *abrupt* faults. Note that most electrochemical SOH estimation algorithms in the existing literature are designed under the assumption that the parameters are slowly-varying and hence may not be readily applicable for *abrupt* fault detection. However, in the proposed diagnostic scheme below, we do not impose any restrictions on the type of fault and hence, can diagnose both types.

FAULT DIAGNOSIS SCHEME

Fault Diagnosis Problem

The fault diagnosis problem addressed here is to detect, and if possible isolate and estimate the faults θ_F, B_F and R_F.

Assumptions and Observations

We make the following assumptions and observations of the system (14)-(18) which will be exploited later in the diagnostic scheme:

Assumption I: The available sensor measurements (voltage, current and temperature) are fault free.

Assumption II: No multiple faults can occur at the same time which means only one of the faults θ_F, B_F and R_F can occur at a time. This assumption enables the isolation of different faults.

Assumption III: The term $h_d = \left(\frac{\partial U^+}{\partial T} - \frac{\partial U^-}{\partial T}\right)$ is constant and known with sufficient accuracy. Although, h_d is generally a function of the surface concentration, the variation in the amplitude of $h_d$is much smaller [36]. In this study, we ignore this small variation and treat h_d as a known constant. As will be seen later, this assumption will facilitate the observer design.

Observation I: The function h is a strictly increasing function of the surface concentration state x_M for any given temperature. Based on this strictly increasing property, given any temperature $T = T^*$, for two points, $x_M^{(1)}$ and $x_M^{(2)}$ in x_M-space, and corresponding points $h^{(1)}\left(x_M^{(1)}, T^*\right)$ and $h^{(2)}\left(x_M^{(2)}, T^*\right)$, we can write:

$$sgn\left(h^{(1)}\left(x_M^{(1)}, T^*\right) - h^{(2)}\left(x_M^{(2)}, T^*\right)\right) = sgn\left(x_M^{(1)} - x_M^{(2)}\right)$$

Diagnostics Scheme

Figure 2 shows the diagnostic scheme. The scheme consists of four observers working in a cascaded manner:

Observer I: Observer I is based on Thermal Model I (17). It receives the measurements of current, voltage and temperature and accurately estimates the open-circuit thermodynamic potential $h(x_M, T)$ even in the presence of the afore-mentioned parametric faults. Its equations are:

$$\begin{aligned} \rho v C_p \dot{\hat{T}}_1 &= -K_h\left(\hat{T}_1 - T_{amb}\right) + u\{-y - \hat{T}_1 h_d\} + L_1 sgn\left(\tilde{T}_1\right) \\ \hat{h}(x_M, T) &= \vartheta_1 / u \end{aligned} \quad (19)$$

where L_1 is the observer gain to be designed, $\hat{T}_1$ is the estimated temperature, $\tilde{T}_1 = T - \hat{T}_1$ and ϑ_1 is a continuous approximation (filtered version) of the switching term $L_1 sgn\left(\tilde{T}_1\right)$.

Observer II: Observer II is based on surface concentration dynamics (15). This observer receives the measured current and estimated thermodynamic potential from Observer I, and in turn accurately estimates the surface concentration even in the presence of the parametric faults and unknown x_1.

$$\begin{aligned} \dot{\hat{\hat{x}}}_M = f_1(T)\theta(A_{22}\hat{\hat{x}}_M) + B_M u \\ + L_2 sgn\left(\vartheta_1/u - h(\hat{\hat{x}}_M, T)\right) \end{aligned} \quad (20)$$

where L_2 is the observer gain to be designed, $\hat{\hat{x}}_M$ is the estimated surface concentration.

Observer III: Observer III is based on the full state Li-ion concentration dynamics given in (14)-(15). This observer receives the measured current and estimated surface concentration from the Observer II, and estimate ϑ_3. This ϑ_3 is then used to estimate the faults θ_F and B_F.

$$\begin{aligned} \dot{\hat{x}}_1 &= f_1(T)\theta\{A_{11}\hat{x}_1 + A_{12}\hat{x}_M\} + L_{31}\tilde{x}_M \\ \dot{\hat{x}}_M &= f_1(T)\theta\{A_{21}\hat{x}_1 + A_{22}\hat{x}_M\} + B_M u + L_{32}\tilde{x}_M + L_{33} sgn(\tilde{x}_M) \\ y_3 &= \vartheta_3 \end{aligned} \quad (21)$$

where L_{31}, L_{32} and L_{33} are the observer gains to be designed, $\hat{x}_1$and $\hat{x}_M$ are the estimated quantities, $\tilde{x}_M = \hat{\hat{x}}_M - \hat{x}_M$ where $\hat{\hat{x}}_M$ is from Observer II, $y_3 = \vartheta_3$ is the output of the Observer III which is a continuous approximation (filtered version) of the switching term $L_{33} sgn(\tilde{x}_M)$.

Observer IV: Observer IV is based on Thermal Model II (18). It receives the measured current, temperature and estimated surface concentration from Observer II, and in turn estimates the fault R_F.

$$\begin{aligned} \rho v C_p \dot{\hat{T}}_4 &= -K_h\left(\hat{T}_4 - T_{amb}\right) \\ &+ u\{-\eta(\hat{x}_M, T, u) + \left(R_{f,ref}\right) f_2(T) u - T h_d\} + L_4 sgn\left(\tilde{T}_4\right) \\ \hat{R}_F &= \vartheta_4 / (f_2(T) u^2) \end{aligned} \quad (22)$$

where L_4 is the observer gain to be designed, $\hat{T}_4$ is the estimated temperature, $\tilde{T}_4 = T - \hat{T}_4$ and ϑ_4 is a continuous approximation (filtered version) of the switching term $L_4 sgn\left(\tilde{T}_4\right)$.

Note: The observers are designed based on sliding mode

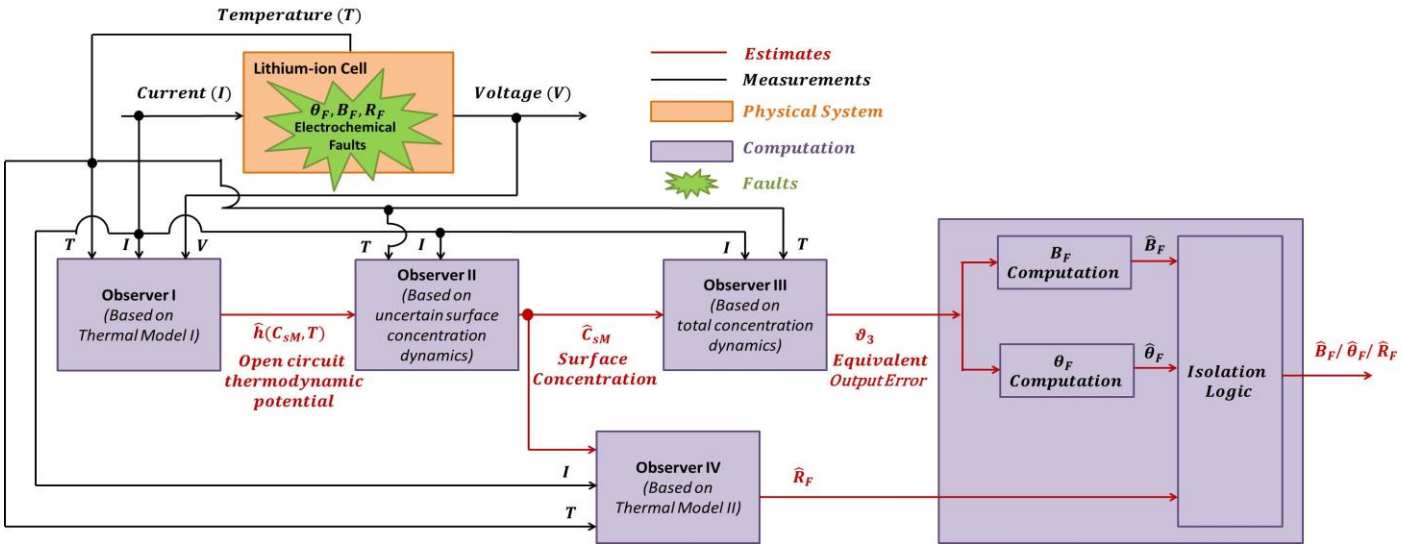

Figure 2: The Fault Diagnosis Scheme

method. In the design of the sliding mode observer, a sliding surface is defined the 'sign' of which is used as the feedback term in the observer [34]. In this paper, the sliding surface is chosen as the origin of the estimation error space for the respective observer. One of the characteristics of sliding mode observers is that for a sufficiently high gain, the convergence to the sliding surface can be guaranteed even in the presence of internal faults. Moreover, after the convergence at the sliding surface, the fault information shows up in the *equivalent output error*, which is the continuous approximation (filtered version) of the switching feedback term in the observer [35].

CONVERGENCE ANALYSIS OF THE OBSERVERS

Before analyzing the convergence of the observers, we define certain quantities that will be used for designing the observer gains. The quantities $|u|_{max}$, $|u^2|_{max}$ are the maximum possible input current and its square and can be determined a priori based on the manufacturer specs. The quantities $|x_M|_{max}$, $|A_{21}x_1|_{max}$ depend on the maximum possible Li-ion concentration inside the battery electrode. These values can also be determined a priori based on the particular electrode chemistry. The values $|h(x_M,T)|_{max}$, $|f_1(T)|_{max}$, $|f_2(T)|_{max}$ are the maximum outputs of the corresponding functions. These values can be predetermined a priori by evaluating the functions in the possible temperature and surface concentration ranges from electrode chemistries and reasonable operating conditions. The values $\left|\tilde{T}_1\right|_{max}$, $\left|\tilde{T}_4\right|_{max}$, $|e|_{max} \triangleq (|x_M - \hat{\tilde{x}}_M|_{max})$, $|A_{21}\tilde{x}_1|_{max}$ and $|\tilde{x}_M|_{max}$ are the maximum estimation errors $\forall t$ for which the observers converge. Essentially these variables define the *region of convergence* in the estimation error spaces. Note that, these values are selected by designers and can be chosen arbitrarily large. The values $|\theta_F|_{max}$ and $|B_F|_{max}$, $|R_F|_{max}$ are the maximum possible amplitude of faults for which the observers will converge. Essentially these variables determine the region in the fault space in which the diagnostic scheme performs satisfactorily. These values are also selected by designers.

Note: The convergence analysis of the observers is done without considering modeling and measurement uncertainties. However, in the simulation studies, we consider these effects while verifying the effectiveness of the scheme.

Convergence Analysis of Observer I

The goal of Observer I is to estimate the thermodynamic potential function $h(x_M,T)$ accurately even in the presence of faults. Subtracting (19) from (17), the error dynamics of the Observer I can be written as:

$$\rho v C_p \dot{\tilde{T}}_1 = -K_h\tilde{T}_1 - u\tilde{T}_1 h_d + uh(x_M,T) - L_1 sgn(\tilde{T}_1) \quad (23)$$

Note that, the sliding surface in this case is $S_1 = \tilde{T}_1 = 0$ as this is inside the 'sign' term. The reachability to this sliding surface S_1 can be analyzed using the Lyapunov function candidate $V_1 = 0.5\rho v C_p S_1^2$. Its derivative is:

$$\dot{V}_1 = \rho v C_p S_1 \dot{S}_1 = \rho v C_p \tilde{T}_1 \dot{\tilde{T}}_1$$

$$\Rightarrow \dot{V}_1 = \tilde{T}_1\{-K_h\tilde{T}_1 - u\tilde{T}_1 h_d + uh(x_M,T) - L_1 sgn(\tilde{T}_1)\}$$

$$\Rightarrow \dot{V}_1 = -K_h\tilde{T}_1^2 - u\tilde{T}_1^2 h_d + \tilde{T}_1 uh(x_M,T) - L_1|\tilde{T}_1| \quad (24)$$

$$\Rightarrow \dot{V}_1 \le -u\tilde{T}_1^2 h_d + \tilde{T}_1 uh(x_M,T) - L_1|\tilde{T}_1|, \text{as } K_h > 0 \quad (25)$$

Now applying the fact $abc \le |a||b||c|$ on the first two terms on the RHS of (25),

$$\dot{V}_1 \le |u||\tilde{T}_1|^2|h_d| + |\tilde{T}_1||u||h(x_M,T)| - L_1|\tilde{T}_1|$$
$$\Rightarrow \dot{V}_1 \le |\tilde{T}_1|\{|u||\tilde{T}_1||h_d| + |u||h(x_M,T)| - L_1\} \quad (26)$$

From (26), we can conclude that for a sufficiently high positive gain L_1 which satisfies the condition $L_1 > |u|_{max}|\tilde{T}_1|_{max}|h_d| + |u|_{max}|h(x_M,T)|_{max}, \forall t, \quad \dot{V}_1 < 0$ and can be written as:

$$\dot{V}_1 \le -\bar{\alpha}_1\sqrt{V_1} \text{ where } \bar{\alpha}_1 = \sqrt{2/\rho v C_p}\{L_1$$
$$-\left(|u|_{max}|\tilde{T}_1|_{max}|h_d| + |u|_{max}|h(x_M,T)|_{max}\right)\} > 0$$

$$\Rightarrow V_1(t) \le \left\{-\frac{\bar{\alpha}_1}{2}t + \sqrt{V_1(t_0)}\right\}^2 \quad (27)$$

From the above analysis, it can be seen that V_1 goes to zero and the sliding surface $S_1 = \tilde{T}_1 = 0$ is reached in finite time defined by $t_1 \le 2\sqrt{V_1(t_0)}/\bar{\alpha}_1$. Considering that we have $S_1 = \tilde{T}_1 = 0$ and $\dot{S}_1 = \dot{\tilde{T}}_1 = 0$ on the sliding surface [34], we can write from (23) that:

$$\vartheta_1 = uh(x_M,T) \quad (28)$$

As mentioned before, $\vartheta_1$is the filtered version of the switching term and can be extracted from the observer by passing $L_1 sgn(\tilde{T}_1)$ through a low-pass filter [34]. Note that, from (28) the thermodynamic potential can be reconstructed as:

$$\hat{h}(x_M,T) = \vartheta_1/u \quad (29)$$

Convergence Analysis of Observer II

The goal of Observer II is to estimate surface concentration state x_M accurately even in presence of faults and unknown x_1. Subtracting (20) from (15), the error dynamics of the Observer II in the presence of faults can be written as:

$$\dot{e} = f_1(T)(\theta + \theta_F)A_{21}x_1 + f_1(T)\theta_F A_{22}x_M$$
$$+f_1(T)\theta A_{22}e + B_F u - L_2 sgn\left(\frac{\vartheta_1}{u} - h(\hat{\tilde{x}}_M,T)\right) \quad (30)$$

where $e = x_M - \hat{\tilde{x}}_M$. Note that, from (29) after the convergence of Observer I we have $\vartheta_1/u = h(x_M,T)$. Therefore, the error dynamics can be written as:

$$\dot{e} = f_1(T)(\theta + \theta_F)A_{21}x_1 + f_1(T)\theta_F A_{22}x_M$$
$$+f_1(T)\theta A_{22}e + B_F u$$
$$- L_2 sgn\left(h(x_M,T) - h(\hat{\tilde{x}}_M,T)\right) \quad (31)$$

From *Observation I*, we can write that:

$$sgn\left(h(x_M,T) - h(\hat{\tilde{x}}_M,T)\right) = sgn(x_M - \hat{\tilde{x}}_M) \quad (32)$$

Considering (32), we can re-write (31) as:

$$\dot{e} = f_1(T)(\theta + \theta_F)A_{21}x_1 + f_1(T)\theta_F A_{22}x_M$$
$$+f_1(T)\theta A_{22}e + B_F u - L_2 sgn(e) \quad (33)$$

Now, the error dynamics can be analyzed using the Lyapunov function candidate $V_2 = 0.5e^2$. The derivative of the Lyapunov function candidate can be written as:

$$\begin{aligned}&\dot{V}_2 = e\dot{e} = e\{f_1(T)(\theta+\theta_F)A_{21}x_1 + f_1(T)\theta_F A_{22}x_M \\ &+f_1(T)\theta A_{22}e + B_F u - L_2 sgn(e) \\ &\Rightarrow \dot{V}_2 = e\{f_1(T)(\theta+\theta_F)A_{21}x_1 + f_1(T)\theta_F A_{22}x_M \\ &+f_1(T)\theta A_{22}e + B_F u\} - L_2 esgn(e)\end{aligned} \quad (34)$$

Applying the fact $abc \le |a||b||c|$ in first term of (34), the following can be written:

$$\begin{aligned}&\dot{V}_2 \le |e|F - L_2|e| \\ &\text{where } F = \{|f_1(T)|(|\theta| + |\theta_F|)|A_{21}x_1| + \\ &|\theta_F||A_{22}||x_M| + |\theta||A_{22}||e| + |B_F|u\}\end{aligned} \quad (35)$$

From (35), we can conclude that for a sufficiently high positive gain L_2 which satisfies the condition:

$L_2 > F_{max} \triangleq |f_1(T)|_{max}(|\theta| + |\theta_F|_{max})|A_{21}x_1|_{max}$
$+|\theta_F|_{max}|A_{22}||x_M|_{max} + |\theta||A_{22}||e|_{max} + |B_F|_{max}u_{max}, \forall t,$
$\dot{V}_2 < 0$ and can be written as:

$$\begin{aligned}&\dot{V}_2 \le -\bar{\alpha}_2\sqrt{V_2} \text{ where} \\ &\bar{\alpha}_2 = L_2 - F_{max} > 0 \\ &\Rightarrow V_2(t) \le \left\{-\frac{\bar{\alpha}_2}{2}t + \sqrt{V_2(t_0)}\right\}^2\end{aligned} \quad (36)$$

From the above analysis, it can be seen that V_2 and therefore e goes to zero in finite time given by $t_2 \le 2\sqrt{V_2(t_0)}/\bar{\alpha}_2$. Therefore, $\hat{\tilde{x}}_M \to x_M$ in finite time.

Convergence Analysis of Observer III

The goal of *Observer III* is to estimate the faults θ_F and B_F. We analyze Observer III under the assumption that Observer II is already converged and provides an accurate estimate of the surface concentration to Observer III. Subtracting (21) from (14) and (15), the error dynamics of Observer I in the presence of faults can be written as:

$$\begin{aligned}\dot{\tilde{x}}_1 &= f_1(T)\{\theta(A_{11}\tilde{x}_1 + A_{12}\tilde{x}_M) + \theta_F(A_{11}x_1 + A_{12}x_M)\} \\ &\quad - L_{31}\tilde{x}_M \\ \dot{\tilde{x}}_M &= f_1(T)\{\theta(A_{21}\tilde{x}_1 + A_{22}\tilde{x}_M) + \theta_F(A_{21}x_1 + A_{22}x_M)\} \\ &+B_F u - L_{32}\tilde{x}_M - L_{33}sgn(\tilde{x}_M)\end{aligned} \quad (37)$$

where $\tilde{x}_M = x_M - \hat{x}_M$ and x_M is available from Observer II. We can analyze the second equation of (37) by choosing a Lyapunov function candidate $V_3 = 0.5\tilde{x}_M^2$. Then:

$$\begin{aligned}&\dot{V}_3 = \tilde{x}_M\dot{\tilde{x}}_M = \tilde{x}_M f_1(T)\theta(A_{21}\tilde{x}_1 + A_{22}\tilde{x}_M) + B_F u\tilde{x}_M \\ &f_1(T)\theta_F(A_{21}x_1 + A_{22}x_M) - L_{32}\tilde{x}_M^2 - L_{33}|\tilde{x}_M| \\ &\Rightarrow \dot{V}_3 \le |\tilde{x}_M|\{|f_1(T)||\theta|(|A_{21}\tilde{x}_1| + |A_{22}||\tilde{x}_M|) \\ &+|f_1(T)||\theta_F|(|A_{21}x_1| + |A_{22}||x_M|) + |B_F||u|\} - L_{33}|\tilde{x}_M| - \\ &L_{32}\tilde{x}_M^2\end{aligned} \quad (38)$$

From (38), we can conclude that for a sufficiently high positive gain L_{33} which satisfies the condition:

$L_{33} > J_{max} \triangleq |f_1(T)|_{max}|\theta|(|A_{21}\tilde{x}_1|_{max} + |A_{22}||\tilde{x}_M|_{max}) +$
$|f_1(T)|_{max}|\theta_F|_{max}(|A_{21}x_1|_{max} + |A_{22}||x_M|_{max}) +$
$|B_F|_{max}|u|_{max}, \forall t,\ \dot{V}_3 < 0.$

The gains L_{31} and L_{32} can be tuned to make sure that under no fault condition ($B_F, \theta_F = 0$), the error $\tilde{x}_1 \to 0$ with a desired fast convergence rate. Therefore, $\dot{V}_3$ can be written as:

$$\begin{aligned}&\dot{V}_3 \le -\bar{\alpha}_3\sqrt{V_3} \text{ where } \bar{\alpha}_3 = L_{33} - J_{max} > 0 \\ &\Rightarrow V_3(t) \le \left\{-\frac{\bar{\alpha}_3}{2}t + \sqrt{V_3(t_0)}\right\}^2\end{aligned} \quad (39)$$

From the above analysis, it can be seen that V_3 and therefore $\tilde{x}_M$ goes to zero in finite time defined by $t_3 \le 2\sqrt{V_3(t_0)}/\bar{\alpha}_3$. Therefore, we have $\tilde{x}_M = 0$ and $\dot{\tilde{x}}_M = 0$ after this finite time. Considering these, (37) can be written as:

$$\begin{aligned}&\dot{\tilde{x}}_1 = f_1(T)\theta(A_{11}\tilde{x}_1) + f_1(T)\theta_F(A_{11}x_1 + A_{12}\hat{x}_M) \\ &0 = f_1(T)\theta(A_{21}\tilde{x}_1) + f_1(T)\theta_F(A_{21}x_1 + A_{22}\hat{x}_M) \\ &\qquad + B_F u - \vartheta_3\end{aligned} \quad (40)$$

where $\vartheta_3$is the filtered version of the switching term and can be extracted from the observer by passing $L_{33}sgn(\tilde{x}_M)$ through a low-pass filter [34]. In the following, we will consider both of the faults separately as by *Assumption II*, their simultaneous occurrence has been excluded.

<u>*Fault 1: B_F fault ($\theta_F = 0$ and $B_F \neq 0$)*</u>

Under this condition, (40) becomes:

$$\begin{aligned}&\dot{\tilde{x}}_1 = f_1(T)\theta(A_{11}\tilde{x}_1) \\ &0 = f_1(T)\theta(A_{21}\tilde{x}_1) + B_F u - \vartheta_3\end{aligned} \quad (41)$$

Note that, all the eigen-values of $f_1(T)\theta A_{11}$ are negative, $\tilde{x}_1 \to 0$ as $t \to \infty$. Therefore, as $t \to \infty$, (41) becomes:

$$\vartheta_3 = B_F u \quad (42)$$

Therefore, the fault can be reconstructed as:

$$\hat{B}_F = \vartheta_3/u \quad (43)$$

<u>*Fault 2: θ_F fault ($\theta_F \neq 0$ and $B_F = 0$)*</u>

Under this condition, (40) becomes:

$$\begin{aligned}&\dot{\tilde{x}}_1 = f_1(T)\theta(A_{11}\tilde{x}_1) + f_1(T)\theta_F(A_{11}\hat{x}_1 + A_{11}\tilde{x}_1 + A_{12}\hat{x}_M) \\ &0 = f_1(T)\theta(A_{21}\tilde{x}_1) \\ &+f_1(T)\theta_F(A_{21}\hat{x}_1 + A_{21}\tilde{x}_1 + A_{22}\hat{x}_M) - \vartheta_3\end{aligned} \quad (44)$$

Note that, in (44) has one algebraic and one differential equation. The unknowns are θ_F and $\tilde{x}_1$. Therefore, we can solve (44) numerically to find the unknowns. The initial condition to this equation can be set to $\tilde{x}_1 = 0$, $\theta_F = 0$ under the assumption that the observer error $\tilde{x}_1$ was sufficiently close to zero before the fault occurs. This can be made sure by properly tuning the gains L_{31} and L_{32}, as mentioned before.

Convergence Analysis of Observer IV

Note that, $\hat{x}_M$ in Observer IV dynamics given in (22) is coming from Observer II and therefore after the convergence of Observer II, we can replace $\hat{x}_M$ by x_M in (22). Now, considering the Observer IV error dynamics by subtracting (22) from (18), we can write that:

$$\rho v C_p\dot{\tilde{T}}_4 = -K_h\tilde{T}_4 + R_F f_2(T)u^2 - L_4 sgn(\tilde{T}_4) \quad (45)$$

Note that, the sliding surface in this case is $S_4 = \tilde{T}_4 = 0$ as this is inside the 'sign' term. The reachability to this sliding surface S_4 can be analyzed using the Lyapunov function candidate $V_4 = 0.5\rho v C_p S_4^2$. The derivative of the Lyapunov function candidate can be written as:

$$\begin{aligned}&\dot{V}_4 = \rho v C_p S_4\dot{S}_4 = \rho v C_p\tilde{T}_4\dot{\tilde{T}}_4 \\ &\Rightarrow \dot{V}_4 = \tilde{T}_4\{-K_h\tilde{T}_4 + R_F f_2(T)u^2 - L_4 sgn(\tilde{T}_4)\} \\ &\Rightarrow \dot{V}_4 = -K_h\tilde{T}_4^2 + \tilde{T}_4 R_F f_2(T)u^2 - L_4|\tilde{T}_4|\end{aligned} \quad (46)$$

$$\Rightarrow \dot{V}_4 \leq \tilde{T}_4 R_F f_2(T) u^2 - L_4 |\tilde{T}_4|, \text{as } K_h > 0 \quad (47)$$

Now, applying the fact $abc \leq |a||b||c|$ on the first term of RHS of (47),

$$\dot{V}_4 \leq |\tilde{T}_4||R_F||f_2(T)||u^2| - L_4|\tilde{T}_4|$$
$$\Rightarrow \dot{V}_4 \leq |\tilde{T}_4|\{|R_F||f_2(T)||u^2| - L_4\} \quad (48)$$

From (48), we can conclude that for a sufficiently high positive gain L_4 which satisfies the condition $L_4 > E_{max} \triangleq |R_F|_{max}|f_2(T)|_{max}|u^2|_{max}, \forall t,\ \dot{V}_4 < 0$ and can be written as:

$$\dot{V}_4 \leq -\bar{\alpha}_4 \sqrt{V_4} \text{ where } \bar{\alpha}_4 = \sqrt{2/\rho v C_p}\{L_4 - E_{max}\} > 0$$

$$\Rightarrow V_4(t) \leq \left\{-\frac{\bar{\alpha}_4}{2} t + \sqrt{V_4(t_0)}\right\}^2 \quad (49)$$

From the above analysis, it can be seen that V_4 goes to zero and the sliding surface $S_4 = \tilde{T}_4 = 0$ is reached in finite time defined by $t_4 \leq 2\sqrt{V_4(t_0)}/\bar{\alpha}_4$. Considering that we have $S_4 = \tilde{T}_4 = 0$ and $\dot{S}_4 = \dot{\tilde{T}}_4 = 0$ in the sliding surface [34], from (23) we can write that:

$$R_F f_2(T) u^2 = \vartheta_4 \quad (50)$$

where ϑ_4 is the filtered version of the switching term and can be extracted from the observer by passing $L_4 sgn(\tilde{T})$ through a low-pass filter [34]. Note that, from (50), the fault can be reconstructed as:

$$\hat{R}_F = \vartheta_4/(f_2(T)u^2) \quad (51)$$

Note: As noticed in the convergence analysis, the estimation of the faults B_F and R_F requires non-zero input current. This is expected because both of these faults enter the battery model by multiplying the input current.

Fault Isolation Logic

Isolation of the faults can be done in the following way: When $\vartheta_4 \neq 0$ and $\vartheta_3 = 0$, then R_F has occurred; when $\vartheta_4 = 0$ and $\vartheta_3 \neq 0$, then either θ_F or B_F has occurred. To isolate θ_F and B_F, the following logic can be used:

Step 1: To isolate exactly which fault has occurred, the applied current through the faulty battery cell should be made zero. This can be achieved either online when the battery is in use if such provision is present in the battery pack (via power electronics circuitry), or offline when the battery is not in use.

Step 2: Note that, in case of no input current $u = 0$, the fault B_F will disappear from the error dynamics equation in (40) thereby making $\vartheta_3 = 0$. However, in case of the occurrence of θ_F fault, $\vartheta_3 \neq 0$ even after $u = 0$. Based on the value of ϑ_3 under the condition $u = 0$, we can isolate these two faults.

Step 3: If the isolation logic above detects a B_F fault, then select the solution of (43) as the fault estimate. If it is θ_F fault, select the solution of (44) as the fault estimate.

RESULTS & DISCUSSIONS

In this section, we demonstrate the effectiveness of the proposed diagnostic scheme via simulation studies. The original SPM with both positive and negative electrode dynamics is used as the plant. It therefore adds some modeling uncertainties to the simulation. The values of the model parameters are adopted from [5] and [36] (6.8 Ah, Metal-Oxide positive electrode and Graphite negative electrode). Moreover, 10 mV and 0.2°C and 10 mA variance noise is added to the voltage, temperature and current measurement, respectively to emulate measurement uncertainties. A particular simulation case study under 1C discharge has been used to verify the potential of the diagnostic observers. The observers are initialized with different initial conditions to verify the convergence. Under this scenario, the performance of the Observer I and II has been shown in Fig. 3. It can be seen that both observers are able to track the open-circuit thermodynamic potential and surface concentration with finite time convergence as mentioned in the previous section.

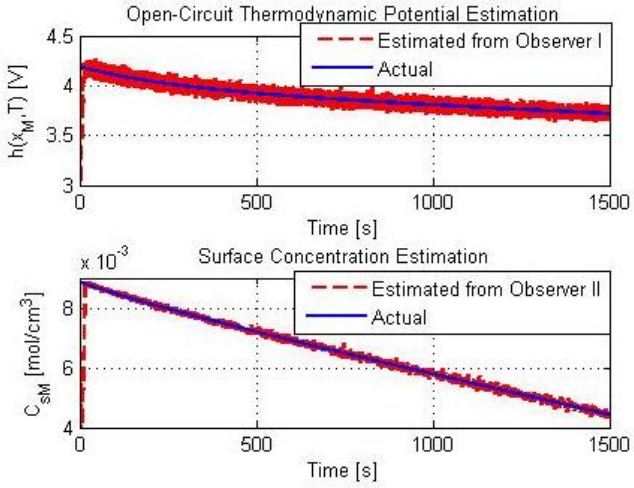

Figure 3: Estimation Performance of Observer I and II

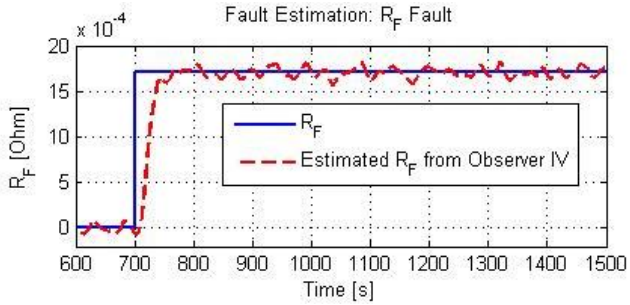

Figure 4: Estimation Performance of Observer IV ($\boldsymbol{R_F}$ fault)

Next, three independent and separate cases have been considered as follows: *Case 1*, A step-like abrupt fault R_F has been injected at 700 sec, *Case 2*, A step-like abrupt fault B_F fault has been injected at 500 sec, *Case 3*: A step-like abrupt fault θ_F fault has been injected at 100 sec. The estimation results are shown in Fig. 4, 5 and 6. From the figures, it can be seen that the diagnostic scheme is able to estimate B_F and R_F with sufficient accuracy. However, there is a considerable amount of steady-state error in θ_F estimation. We have noted in our simulation studies that θ_F fault estimation is more sensitive

to the modeling uncertainties than the other two faults. This is because this fault is multiplied with the states of the system, therefore, the state estimation error under modeling uncertainties add more error to the estimate of this fault.

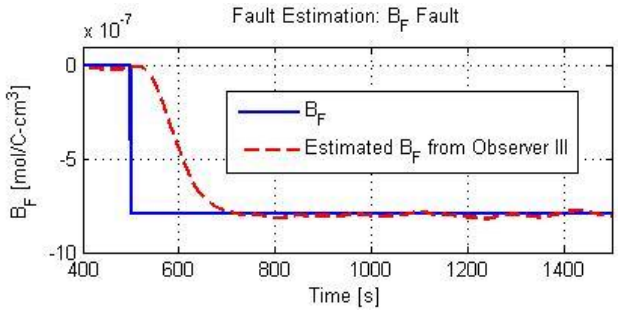

Figure 5: Estimation Performance of Observer III ($\boldsymbol{B_F}$ fault)

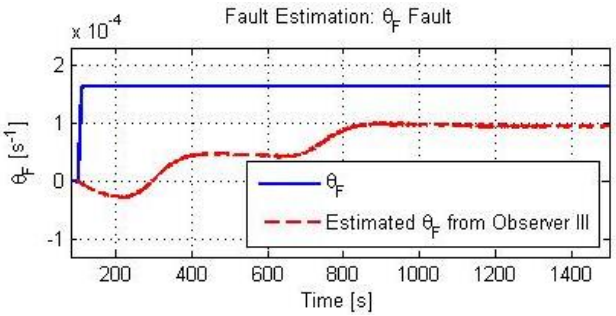

Figure 6: Estimation Performance of Observer III ($\boldsymbol{\theta_F}$ fault)

CONCLUSION

In this paper, an observer-based fault diagnosis scheme is presented that can detect, isolate and estimate a few electrochemical faults in Li-ion batteries. A reduced order electrochemical-thermal model of the Li-ion cell is used where the electrochemical faults are modelled as parametric/multiplicative faults in the system. The designs of the observers are done based on the sliding mode methodology. Convergence of the observers is verified along with the design of the observer gains via Lyapunov's direct method. The effectiveness of the fault diagnosis scheme is tested via simulation studies and it is found that the fault diagnosis scheme is able to detect, isolate and estimate the injected parametric faults.

However, there are some issues that should be considered in future extension to this work. The design of the fault diagnosis scheme should explicitly consider the effect of the modeling uncertainties to improve the robustness of the scheme. Finally, the scheme should be validated with experimental studies. To do this study, different experimental test cases should be designed that capture the effect of different electrochemical faults in a physical battery.

ACKNOWLEDGMENTS

This research is supported by the US Department of Energy GATE program under grant number DE-EE0005571.

REFERENCES

[1] Saha, B., Goebel, K., Poll, S., and Christophersen, J., 2007. "An integrated approach to battery health monitoring using bayesian regression and state estimation". In 2007 IEEE Autotestcon, pp. 646-653.

[2] Ng, K. S., Moo, C., Chen, Y., and Hsieh, Y., 2009. "Enhanced coulomb counting method for estimating state-of-charge and state-of-health of lithium-ion batteries". *Applied Energy*, vol. 86, no. 9, pp. 1506-1511.

[3] Plett, G. L., 2004. "Extended Kalman filtering for battery management systems of LiPB-based HEV battery packs: Part 3. State and parameter estimation". *Journal of Power sources*, vol. 134, no. 2, pp. 277-292.

[4] Kim, Il-Song, 2010. "A Technique for Estimating the State of Health of Lithium Batteries Through a Dual-Sliding-Mode Observer". *IEEE Transactions on Power Electronics*, vol.25, no.4, pp.1013-1022.

[5] Smith, K. A., Rahn, C. D., and Wang, C., 2010. "Model-based electrochemical estimation and constraint management for pulse operation of lithium ion batteries". *IEEE Transactions on Control Systems Technology*, vol. 18, no. 3, pp. 654-663.

[6] Klein, R.; Chaturvedi, N.A.; Christensen, J.; Ahmed, J.; Findeisen, R.; Kojic, A., 2013. "Electrochemical Model Based Observer Design for a Lithium-Ion Battery". *IEEE Transactions on Control Systems Technology*, vol.21, no. 2, pp. 289-301.

[7] Santhanagopalan, S., and White, R. E., 2006. "Online estimation of the state of charge of a lithium ion cell". *Journal of Power Sources*, vol. 161, no. 2, pp. 1346-1355.

[8] Domenico, D., Stefanopoulou, A., and Fiengo, G., 2010. "Lithium-ion battery state of charge and critical surface charge estimation using an electrochemical model-based extended Kalman filter". *ASME Journal of Dynamic Systems, Measurement, and Control*, vol. 132, no. 6, pp. 061302.

[9] Moura, S. J., Chaturvedi, N. A., and Krstic, M., 2012. "PDE estimation techniques for advanced battery management systems—Part I: SOC estimation". In 2012 American Control Conference (ACC), pp. 559-565.

[10] Samadi, M. F., Alavi, S. M., and Saif, M., 2013. "Online state and parameter estimation of the Li-ion battery in a Bayesian framework". In 2013 ACC, pp. 4693-4698.

[11] Wang, Y., Fang, H., Sahinoglu, Z., Wada, T. and Hara, S., 2014. "Adaptive Estimation of the State of Charge for Lithium-Ion Batteries: Nonlinear Geometric Observer Approach," In IEEE Transactions on Control Systems Technology, available online.

[12] Fang, H., Wang, Y., Sahinoglu, Z., Wada, T., and Hara, S., 2014. "State of charge estimation for lithium-ion batteries: An adaptive approach". Control Engineering Practice, vol. 25, pp. 45-54.

[13] Dey, S., and Ayalew, B., 2014. "Nonlinear Observer Designs for State-of-Charge Estimation of Lithium-ion Batteries". In 2014 American Control Conference (ACC), pp. 248-253.

[14] Dey, S., Ayalew, B., and Pisu. P., 2014. “Nonlinear Robust Observers for State-of-Charge Estimation of Lithium-ion Cells Based on a Reduced Electrochemical Model”. IEEE Transactions on Control System Technology, available online, DOI: 10.1109/TCST.2014.2382635.

[15] Dey, S., Ayalew, B., and Pisu, P., 2014. “Combined estimation of State-of-Charge and State-of-Health of Li-ion battery cells using SMO on electrochemical model.” In 13th International Workshop on VSS, pp. 1-6.

[16] Dey, S., Ayalew, B., and Pisu, P., 2014. “Adaptive Observer Design for a Li-Ion Cell Based on Coupled Electrochemical-Thermal Model.” In ASME 2014 Dynamic Systems and Control Conference.

[17] Arora, P., White, R. E., and Doyle, M., 1998. “Capacity fade mechanisms and side reactions in lithium-ion batteries”. In Journal of Electrochemical Society, vol. 145, no. 10, pp. 3647–3667.

[18] Aurbach, D., Zinigrad, E., Cohen, Y., and, Teller, H., 2002. “ A short review of failure mechanisms of lithium metal and lithiated graphite anodes in liquid electrolyte solutions”. In Solid State Ionics, vol. 148, pp. 405–416.

[19] Alavi, S. M., Samadi, M., and Saif, M., 2013. “Diagnostics in Lithium-Ion Batteries: Challenging Issues and Recent Achievements”. In Integration of Practice-Oriented Knowledge Technology: Trends and Prospectives, Springer Berlin Heidelberg, pp. 277-291.

[20] Marcicki, J., Onori, S., and Rizzoni, G., 2010. “Nonlinear fault detection and isolation for a lithium-ion battery management system”. In ASME 2010 Dynamic Systems and Control Conference, pp. 607-614.

[21] Singh, A., Izadian, A., and Anwar, S., 2013. “Fault diagnosis of Li-Ion batteries using multiple-model adaptive estimation”. In IECON 2013, pp. 3524-3529.

[22] Mukhopadhyay, S., and Zhang, F., 2012. “Adaptive detection of terminal voltage collapses for li-ion batteries”. In IEEE 51st CDC, pp. 4799 – 4804.

[23] Chen, W., Chen, W. T., Saif, M., Li, M. F., and Wu, H., 2014. “Simultaneous Fault Isolation and Estimation of Lithium-Ion Batteries via Synthesized Design of Luenberger and Learning Observers”. In IEEE Transactions on Control Systems Technology, vol.22, no.1, pp. 290-298.

[24] Lombardi, W., Zarudniev, M., Lesecq, S., and Bacquet, S., 2014. “Sensors fault diagnosis for a BMS”. In 2014 European Control Conference (ECC), pp. 952-957.

[25] Liu, Z., Ahmed, Q., Rizzoni, G., and He, H., 2014. “Fault Detection and Isolation for Lithium-Ion Battery System Using Structural Analysis and Sequential Residual Generation”. In the Proceedings of 2014 ASME Dynamic Systems and Control Conference (DSCC),.

[26] Alavi, S. M., Samadi, M. F., and Saif, M., 2013. “Plating Mechanism Detection in Lithium-ion batteries, by using a particle-filtering based estimation technique”. In 2013 ACC, pp. 4356 - 4361.

[27] Zhou, X., Ersal, T., Stein, J. L., and Bernstein, D. S., 2014. “Battery State of Health Monitoring by Side Reaction Current Density Estimation via Retrospective-Cost Subsystem Identification”. In ASME 2014 Dynamic Systems and Control Conference.

[28] Dey, S., Mohon, S., Pisu, P., and Ayalew, B., 2015. “Sensor Fault Detection, Isolation and Estimation in Lithium-ion Batteries”. In preparation, IEEE Transactions on Control Systems Technology.

[29] Nuhic, A., Terzimehic, T., Soczka-Guth, T., Buchholz, M.,and Dietmayer, K., 2013. “Health diagnosis and remaining useful life prognostics of lithium-ion batteries using data-driven methods”. In Journal of Power Sources, vol. 239, no.0,pp. 680 – 688.

[30] Wang, D., Miao, Q., and Pecht, M., 2013. “Prognostics of lithium-ion batteries based on relevance vectors and a conditional three-parameter capacity degradation model”. In Journal of Power Sources, vol. 239, no. 0, pp. 253–264.

[31] Kozlowski, J., 2003. “Electrochemical cell prognostics using online impedance measurements and model-based data fusion techniques”. In Aerospace Conference, 2003. Proceedings. 2003 IEEE, Vol. 7, pp. 3257–3270.

[32] Muddappa, V. K. S., Anwar, S., 2014. “Electrochemical Model Based Fault Diagnosis of Li-ion Battery Using Fuzzy Logic,” In ASME 2014 IMECE.

[33] Chaturvedi, N. A., Klein, R., Christensen, J., Ahmed, J., and Kojic, A., 2010. “Algorithms for Advanced Battery-Management Systems”. *IEEE Control Systems Magazine*, vol.30, no.3, pp.49-68.

[34] Utkin, V., Guldner, J., and Shi, J., 1999. *Sliding mode control in electromechanical systems*. CRC press.

[35] Edwards, C., Spurgeon, S. K., and Patton, R. J., 2000. “Sliding mode observers for fault detection and isolation”. In Automatica, vol. 36, no. 4, pp. 541-553.

[36] Guo, M., Sikha, G., and White, R.E., 2011. “Single-particle model for a lithium-ion cell: thermal behavior”. *Journal of The Electrochemical Society*, vol. 158, no. 2, pp. A122-A132.

[37] Tanim, T. R., Rahn, C. D., and Wang, C. Y., 2014. “A Temperature Dependent, Single Particle, Lithium Ion Cell Model Including Electrolyte Diffusion,” In ASME Journal of Dynamic Systems, Measurement, and Control.

[38] Lin, X., Perez, H. E., Siegel, J. B., Stefanopoulou, A. G., Li, Y., Anderson R. D., Ding, Y., and Castanier, M. P., 2013. "Online Parameterization of Lumped Thermal Dynamics in Cylindrical Lithium Ion Batteries for Core Temperature Estimation and Health Monitoring". IEEE Transactions on Control Systems Technology, vol.21, no.5, pp.1745-55.

[39] Gertler, Janos, 1998. *Fault detection and diagnosis in engineering systems*. CRC press.

[40] Siegel, J. B., Lin, X., Stefanopoulou, A. G., Hussey, D. S., Jacobson, D. L., and Gorsich, D., 2011. “Neutron imaging of lithium concentration in LFP Pouch cell battery”. Journal of the Electrochemical Society, vol.158, no.5, pp. A523 – A529.